

Using Carbon Dioxide for Subsea Long-Duration Energy Storage

Charise Cutajar * , Tonio Sant  and Luke Jurgen Briffa

Department of Mechanical Engineering, University of Malta, 2080 Msida, Malta; tonio.sant@um.edu.mt (T.S.); luke.j.briffa.17@um.edu.mt (L.J.B.)

* Correspondence: charise.cutajar@um.edu.mt

Abstract: This paper investigates the operating benefits and limitations of utilizing carbon dioxide in hydro-pneumatic energy storage systems, a form of compressed gas energy storage technology, when the systems are deployed offshore. Allowing the carbon dioxide to transition into a two-phase fluid will improve the storage density for long-duration energy storage. A preliminary comparative study between an air-based and a carbon dioxide-based subsea hydro-pneumatic energy storage system is first presented. The analysis is based on thermodynamic calculations assuming ideal isothermal conditions to quantify the potential augmentation in energy storage capacity for a given volume of pressure containment when operating with carbon dioxide in lieu of air. This is followed by a transient thermal analysis of the carbon dioxide-based hydro-pneumatic energy storage system, taking into account the real scenario of a finite thermal resistance for heat exchange between the gas and the surrounding seawater. Results from numerical modelling revealed that the energy storage capacity of a carbon dioxide-based subsea hydro-pneumatic energy storage system operating under ideal isothermal conditions can be theoretically increased by a factor of 2.17 compared to an identical air-based solution. The numerical modelling revealed that, under real conditions under which transient effects resulting from a finite thermal resistance are accounted for, the achievable factor is lower, depending on the charging and discharging time, the initial temperature, and whether a polyethylene liner for corrosion prevention is considered or not.

Keywords: subsea; energy storage; carbon dioxide; liquefaction; thermodynamics; transient thermal



Citation: Cutajar, C.; Sant, T.; Briffa, L.J. Using Carbon Dioxide for Subsea Long-Duration Energy Storage. *Gases* **2024**, *4*, 295–309. <https://doi.org/10.3390/gases4030017>

Academic Editor: Paola Ammendola

Received: 9 August 2024

Revised: 8 September 2024

Accepted: 16 September 2024

Published: 18 September 2024



Copyright: © 2024 by the authors. Licensee MDPI, Basel, Switzerland. This article is an open access article distributed under the terms and conditions of the Creative Commons Attribution (CC BY) license (<https://creativecommons.org/licenses/by/4.0/>).

1. Introduction

Long-duration energy storage (LDES) systems are becoming a critical means for safeguarding the reliability and flexibility of power systems, for a high penetration of intermittent renewables, such as wind and solar power, into the grid. Compressed air energy storage (CAES) systems [1], in particular hydro-pneumatic energy storage (HPES) solutions [2,3], have been favoured due to their high thermal efficiencies and ability to deploy at sea for co-location with offshore renewable energy parks.

Despite the simplicity of operation, the large volume requirements of HPES systems have been identified as a major technical and financial barrier to achieving the required storage capacities. Recently, the idea of utilizing carbon dioxide (CO₂) in lieu of air has been regarded as an attractive opportunity to increase the energy storage densities (ESDs) of HPES systems.

Liquid CO₂ energy storage (LCES) has been gaining interest due to the favourable thermo-physical properties of CO₂ that allow the gas to be liquefied and stored at relatively low pressures (i.e., <73.8 bar) and ambient temperatures (i.e., <304.25 K) [4], thus driving significant cost reductions associated with the pressure containment of the storage system. Moreover, liquefying CO₂ rather than liquefying air itself prevents the necessity of dealing with the cryogenic temperatures (i.e., <83.15 K) linked to liquid air energy storage (LAES) [5]. In addition, the limited ESDs of HPES systems can be effectively increased upon condensation of the CO₂ gas. A gas like air, which does not condensate during operation, limits the liquid-piston travel, and thus the amount of energy stored. Conversely, with the

gas undergoing phase change and partially liquefying, the accumulator volume that can be exploited for energy storage is maximized.

Counter-arguments about using CO₂ in HPES systems have been linked to the costly corrosion mitigation measures required, especially when considering offshore energy storage. The condensation of CO₂ on low-carbon steels typically used for offshore accumulators is highly corrosive in the presence of seawater. The reaction involves the formation of carbonic acid (H₂CO₃) which results in a pitting attack on the steel. Consequently, reliable corrosion preventive measures like anti-corrosion paint and/or linings would be necessary. For example, high-density polyethylene (HDPE) liners are widely used in oil and gas pipelines due to the enhanced corrosion resistivity offered at competitive prices. Yet, when tested for offshore HPES applications [6], HDPE liners were reported to significantly lower the thermal efficiency of operation due to low thermal conductivity [6]. A further difficulty is the high solubility of CO₂ in water, whereby the liquid-piston mechanism of a CO₂-based HPES system will fail unless a diaphragm which separates the two fluids, seawater and CO₂, is present. A separator, similar to a pipeline inspection gauge (PIG), which is already widely used in the pipeline industry, would be an effective way to create a partition between the distinct fluid bodies [6].

Several analyses [7–9] have been conducted to quantify the augmented storage capacities when shifting from conventional CAES systems to LCES, and values up to 2.8 times were reported in the literature [9]. The quoted value is however dependent on the systems being considered. In [7–9], the investigations were limited to onshore-based systems or storage of air/liquid CO₂ in aquifers [7,8], both of which demand complex thermal energy storage techniques that inflate the size and cost of the system. Commercially, CO₂ is already being exploited for energy storage by what is known as the CO₂ Battery, currently under development by Energy Dome [10]. The operation of the onshore LDES plant is able to sustain the provision of electricity for up to 10 h with round-trip efficiencies being claimed to be above 75% [10].

More pertinent to the scope of the present research is, however, the utilization of CO₂ undergoing phase change in HPES systems operating in a closed-cycle configuration. Yet, research in this specific field is somewhat limited. Abu-Heiba et al. [11] investigated the potential increase in the storage capacity of what is known as the GLIDES solution by almost fully replacing air in the system with CO₂. The ESD of the GLIDES system was reported to be augmented by 56.8% (or an augmentation factor of 1.568) from 4.67 MJ/m³ (i.e., 1.30 kWh/m³) when using pure nitrogen (N₂) representing air to 7.33 MJ/m³ (i.e., 2.04 kWh/m³) when using a mixture of 88% CO₂ and 12% N₂.

In a previous work, Cutajar et al. [12] investigated the potential increase in the ESD of subsea HPES systems when operating with CO₂ in place of air. The analyses were limited to isothermal considerations only, with the transient effects resulting from a finite thermal resistance to heat transfer between the compressible fluid storing the energy and the surrounding seawater being ignored. The study [12] revealed that CO₂ can theoretically provide up to three times the ESD of an equivalent air-based HPES system. The augmentation factor was, however, observed to vary with several parameters including the operating pressure ratio, sea depth, initial fluid temperature, and extent of CO₂ liquefaction (i.e., the dryness fraction).

Briffa et al. [6] investigated subsea CO₂-based HPES systems in more detail by modelling the transient effects resulting from thermal resistances. It was estimated that the use of CO₂ in lieu of air boosted the energy storage capacity (ESC) by up to 55.2%. However, the investigations also revealed that the air-based system was much more efficient, reaching round-trip thermal efficiencies beyond 90%. Contrastingly, the CO₂-based alternative attained thermal efficiencies between 78 and 87% [6].

This paper extends the work of Cutajar et al. [12] and Briffa et al. [6] by investigating different operating conditions of an offshore HPES system. Situating the system subsea addresses the challenge of land constraints whilst enhancing the thermal efficiency during operation due to the surrounding seawater environment which acts as an excellent heat sink

during charging (compression) and as a heat source during discharging (expansion). The study employs (i) the ideal isothermal thermodynamic and (ii) transient thermal models from [12] and [6], respectively, to investigate further potential benefits and limitations of utilizing CO₂ for subsea HPES systems which have not yet been explored in [6,12]. This study aims to narrow the knowledge gap in terms of subsea HPES systems operating on CO₂ as the energy storage medium. The investigations conducted thus far [6–9,11,12] fall short of indicating the main factors that contribute to the liquefaction of CO₂, which is essential to achieve higher ESCs. By analyzing the thermal performance of the CO₂-based unit, the parameters governing the efficiency and the ESC of the system are identified. Therefore, a better comparison can be made to the air-based unit, highlighting the prominent differences introduced by a change in the compressible fluid.

The mathematical groundwork for the two distinct numerical models is reviewed in Section 2, followed by the description of the research approach adopted in Section 3. The results obtained from the two models and interpretation of plots thereof are presented in Section 4. Finally, the key and novel findings are highlighted in Section 5 together with suggestions for future work.

2. Mathematical Models

Figures 1 and 2 illustrate the two HPES systems being investigated in the present study. Both systems are considered to be geometrically identical pipelines exposed to the same subsea conditions. The only difference is that HPES-1 operates with air as the energy storage medium, whereas HPES-2 utilizes CO₂ for storing energy. Note that, for the present study, the sea depth Z_{sw} was maintained constant at 10.5 m while including the effect of hydrostatic pressure in the analysis.

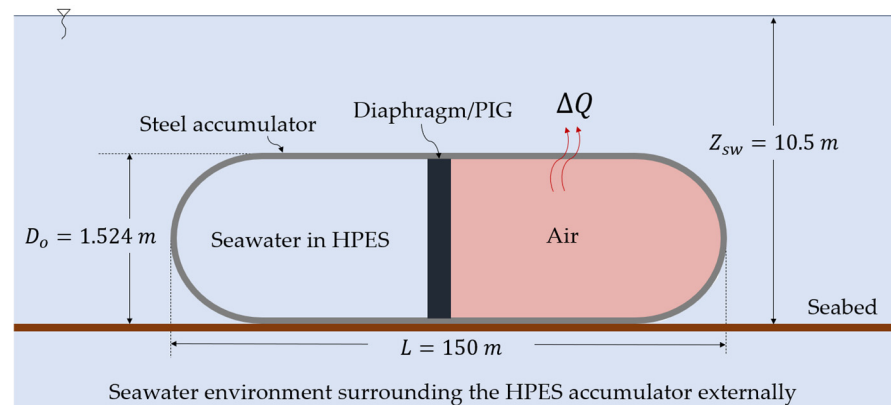


Figure 1. Subsea HPES system under investigation: air-based HPES-1 (not to scale).

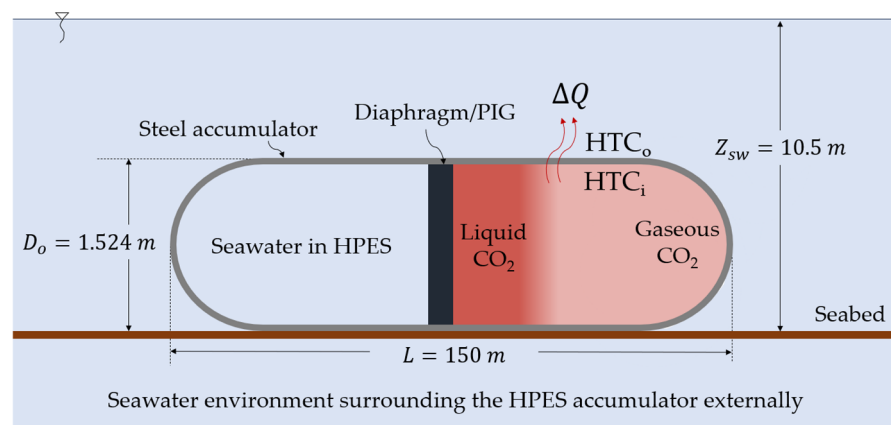


Figure 2. Subsea HPES system under investigation: CO₂-based HPES-2 (not to scale).

A PIG is included in both HPES systems to act as a diaphragm. For HPES-1, the PIG is important to prevent the dilution of the compressed air into the seawater. For HPES-2, the PIG is compulsory for the purpose explained in Section 1. Furthermore, the thermodynamic and transient thermal models put forward in Sections 2.1 and 2.2, respectively, both assume a horizontal liquid-piston travel. Thus, the seawater–PIG–compressible fluid interface is considered to be vertical, as depicted in Figures 1 and 2.

The systems operate on the fundamental concept of closed-gas HPES solutions. A pump is driven by excess renewable energy to pump seawater inside the subsea accumulator which is pre-charged with air or CO₂. The injection of seawater inside the pressure containment system causes the other fluid to compress (and condense in the case of CO₂). Thus, the HPES system is said to be charging and energy storage takes place. Recovering the stored energy requires discharging the system by expelling the seawater out through a hydraulic turbine and allowing the compressed fluid to expand back (and evaporate in the case of CO₂). The turbine would then drive a generator, supplying electricity to the grid. It is worth emphasizing that neither the air nor the CO₂ flow through the hydraulic circuit, but are simply enclosed within the accumulator.

2.1. Thermodynamic Model for Ideal Isothermal Conditions (CO₂HPES Model)

The thermodynamic model CO₂HPES [12] aims to quantify the difference in the ideal energy storage capacity ESC_i between the two subsea HPES systems: HPES-1 operating with air and HPES-2 utilizing CO₂. The model is based on the assumption that the compression and expansion processes occur in an ideal isothermal manner and the thermal resistance to heat transfer between the compressible fluid and the surrounding seawater is neglected. Furthermore, air in HPES-1 is treated as a dry, ideal gas, whereas the CO₂ in HPES-2 is considered to always exist at superheated or dry conditions at the initial working state, yet changes phase during the compression/expansion process.

The ESC_i of an HPES system in kilowatt hours (kWh) is derived from the work done ΔW_i in Joules (J) during isothermal compression/expansion via Equation (1):

$$ESC_i = \Delta W_i / (3.6 \times 10^6) \quad (1)$$

In turn, the thermodynamic work ΔW_i can be evaluated by applying the energy conservation principle:

$$\Delta W_i = \Delta Q - \Delta U \quad (2)$$

where ΔQ is the heat exchange and ΔU is the change in internal energy of the system, both in J. For air as an ideal, single-phase gas, Equation (2) transforms into

$$ESC_i (\text{air}) = \Delta W_i (\text{air}) / (3.6 \times 10^6) = \{ [p_f v_f m_{\text{air}} \ln(r_p)] - \{ p_{\text{hyd}} v_f m_{\text{air}} (r_p - 1) \} \} / (3.6 \times 10^6) \quad (3)$$

In Equation (3), p_f and v_f are the final air pressure in Pascals (Pa) and specific volume in cubic metres per unit mass (m³/kg), respectively. Moreover, m_{air} is the mass of air in HPES-1 in kilograms (kg) and r_p is the operating pressure ratio. Also, p_{hyd} is the hydrostatic pressure. Indeed, the second term in curly {} brackets on the right-hand side of Equation (3) represents the work done against hydrostatic pressure, which has to be accounted for in a subsea energy storage system.

Conversely, for CO₂ undergoing a phase change, ΔQ is represented by a change in the specific entropy s (in J/kg K) of the fluid:

$$\Delta Q = m_{\text{CO}_2} T \Delta s = m_{\text{CO}_2} T (s_f - s_0) \quad (4)$$

and ΔU is expressed as the change in the specific enthalpy h (in J/kg) of the fluid:

$$\Delta U = m_{\text{CO}_2} [(h_f - h_0) - (p_f v_f - p_0 v_0)] \quad (5)$$

Therefore, for CO₂, Equation (2) transposes into

$$ESC_i(\text{CO}_2) = \Delta W_i(\text{CO}_2)/(3.6 \times 10^6) = [m_{\text{CO}_2}/3.6 \times 10^6] \{ [T(s_f - s_0)] - \{ (h_f - h_0) - (p_f v_f - p_0 v_0) \} \} \quad (6)$$

For a complete derivation, reference can be made to the previous work by the authors in [12]. In Equations (4)–(6), m_{CO_2} is the mass of CO_2 in HPES-2, which, despite a phase change, remains constant by the conservation of mass principle. Moreover, T is the operating temperature in Kelvin (K), which is maintained unchanged under the assumed isothermal conditions. The subscripts 0 and f indicate the initial and final stages of compression, respectively, where the CO_2 changes from a dryness fraction of $x = 1$ to being completely liquefied at $x = 0$.

The extent of increase in ESC_i when compressing CO_2 instead of air could thus be determined from the augmentation factor α :

$$\alpha = ESC_i(\text{CO}_2)/ESC_i(\text{air}) \quad (7)$$

2.2. Transient Thermal Model (C_2O_2 Model)

The transient thermal model C_2O_2 [6] is also based on the energy conservation law defined in Equation (2). However, the model incorporates the thermal resistance to heat transfer between the compressible fluid and the surrounding seawater, thus accounting for transient effects. The model is thus able to capture the conditions when the HPES compression and expansion processes deviate from the ideal (i.e., isothermal) behaviour. Therefore, to cater to temperature changes, instead of Equation (6), which assumed isothermal conditions, Equation (2) is modified into

$$\Delta W_r(\text{CO}_2)/(3.6 \times 10^6) = [\{\Delta Q - (m_{\text{CO}_2} C_v \Delta T)\} - W_f] [1/(3.6 \times 10^6)] \quad (8)$$

In Equation (8), ΔW_r is the real work done under non-isothermal conditions. Moreover, C_v is the specific heat capacity at constant volume in J/kg K and ΔT is the change in fluid temperature during operation. The term W_f accounts for the work lost against the frictional forces in moving the PIG along the pipeline.

For the computation of ΔQ , only the cylindrical surface area in contact with CO_2 is considered (refer to Figure 2) to be the predominant interface for heat exchange to occur. The correlations for the Nusselt (Nu) number to compute the external and internal heat transfer coefficients HTC_o and HTC_i (refer to Figure 2) depend on several factors, including whether the location of interest is internal or external to the accumulator, and the type of convective flow (i.e., free or forced). For the two-phase transition region of CO_2 , empirical correlations are distinguished in terms of whether the fluid is condensing (as is the case during the charging cycle of HPES-2) or evaporating (which occurs during the discharging period of HPES-2). The correlations developed by various scholars as utilized in C_2O_2 [6] in the present study are listed in Tables 1 and 2 and may be reviewed in full detail from the respective sources [13–18].

Table 1. Correlations implemented in C_2O_2 [6] to determine the Nu number for single-phase fluids.

Location	HTC	Type of Convection	Fluid	HTC
External	HTC_o	Free	Seawater	Churchill-Chu [13]
External	HTC_o	Forced	Seawater	Churchill-Bernstein [14]
Internal	HTC_i	Free	Gaseous CO_2	Ludovisi-Garza [15]
Internal	HTC_i	Forced	Gaseous CO_2	Gnielinski [16]

The HTC during operation could then be computed via Equation (9), with k being the thermal conductivity of CO_2 and D the (internal or external) diameter of the accumulator. The ΔQ in Equation (8) could thus be determined through a thermal network, accounting

for convective effects internal and external to the accumulator, in series with the conductive heat transfer mechanism across the thickness of the steel wall of the accumulator.

$$HTC = Nu(k/D) \quad (9)$$

Table 2. Correlations implemented in C₂O₂ [6] to determine the Nu number for two-phase CO₂.

Location	HTC	Fluid	Phase Change Mode	HTC
Internal	HTC _i	Two-phase CO ₂	Condensing	Thome et al. [17]
Internal	HTC _i	Two-phase CO ₂	Evaporating	Fang et al. [18]

Equation (8) was employed separately for the charging and discharging process to obtain the real work done during each process ΔW_{r-c} (CO₂) and ΔW_{r-d} (CO₂), respectively. The former parameter was considered to also reflect the real ESC under real operating conditions. In mathematical terms and analogous to Equation (6),

$$ESC_r(\text{CO}_2) = \Delta W_{r-c}(\text{CO}_2) / (3.6 \times 10^6) \quad (10)$$

The thermal efficiency η could thus be defined as the ratio of the actual energy (or work) recovered during discharging ΔW_{r-d} (CO₂) as compared to the work done (i.e., energy stored) during charging ΔW_{r-c} (CO₂):

$$\eta = \Delta W_{r-d}(\text{CO}_2) / \Delta W_{r-c}(\text{CO}_2) \quad (11)$$

Solving for Equations (8) and (10) also allows for an ESC factor β to be established as a measure of how close the real ESC is to the ideal scenario estimated from the thermodynamic model outlined in Section 2.1. In other words,

$$\beta = ESC_r(\text{CO}_2) / ESC_i(\text{CO}_2) \quad (12)$$

Values of η and β close to unity imply exceptional operating conditions approximating the ideal isothermal scenario.

3. Methodology

Figure 3 illustrates the overall research approach undertaken and how the different numerical models were executed to converge towards the research goals. The mathematical models described in Section 2 were implemented into two distinct numerical codes in Python© Version 3.7 [19]. The properties of air and CO₂ (as applicable) were derived from the in-built Python© library CoolProp. Validation procedures were conducted for both numerical models. The numerical outcomes from CO2HPES [12] for parameters including the ideal energy storage capacity ESC_i (CO₂), the enthalpy h , the entropy s , and other fluid parameters were always within $\pm 0.30\%$ of analytical results. Further information may be found in [6,12].

For the thermodynamic analysis, the sizing of the accumulator for the air-based HPES system HPES-1 was derived from the optimization algorithm SmartPVB [20]. The latter was specifically developed to yield optimum structural design (i.e., maximize the ESC per unit mass of steel requirement for the accumulator) and operating parameters for offshore HPES accumulators operating with air as the energy storage medium. The geometric parameters of HPES-1 were then input into the model CO2HPES [12] to analyze the operation of HPES-2. In other words, the same accumulator was modelled to operate with CO₂ undergoing phase change in lieu of air. The difference between HPES-1 and HPES-2 in terms of thermodynamic parameters could thus be identified, as discussed in Section 4.1.

For the transient thermal analysis conducted using the model C₂O₂ [6], only HPES-2 was considered. The equations described in Section 2.2 were systemized in a time-marching

approach to model charging–hold–discharging–hold periods t that fall under LDES criteria (i.e., >6 h). A total of twelve different simulations were executed to identify the parameters which highly influenced the operation, as outlined in Section 4.2. The parameters for the sensitivity analysis were chosen to reproduce new data sets for interpretation that were not considered in previous works [6,12].

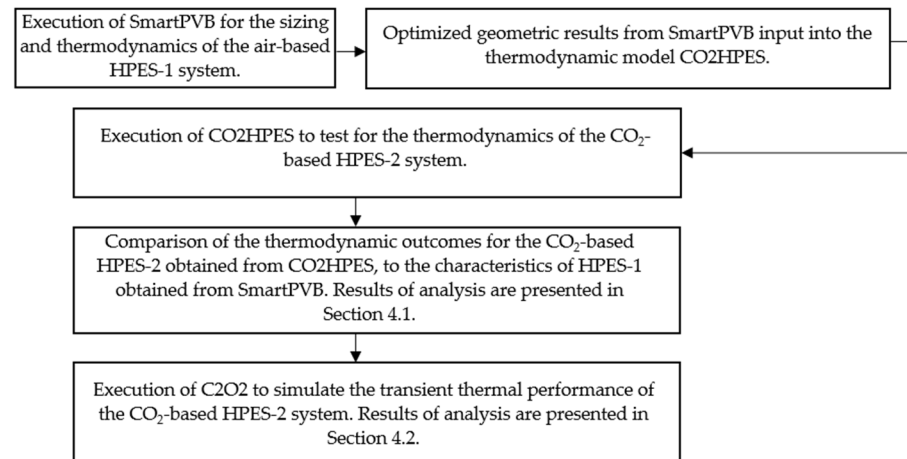


Figure 3. Flowchart illustrating overall research approach [6,12,20].

Test conditions and outcomes from both analyses are presented in the upcoming section together with a detailed discussion.

4. Results and Discussion

4.1. Results from Thermodynamic Analysis Assuming Ideal Isothermal Conditions

For the parametric thermodynamic analysis, only the operating pressure ratio r_p was varied with assumed values of 1.5, 2.5, and 3.5, since a detailed parametric investigation had already been performed and is documented in [12].

Table 3 presents the comparison between the air-based HPES-1 and the CO₂-based HPES-2 at an optimum r_p of 1.5. The operating conditions for the two HPES systems were maintained the same except that the compressible fluid was air for the former and CO₂ for the latter system. In fact, HPES-1 shall serve as a reference model with respect to HPES-2, to identify the differences arising due to a change in the energy storage fluid.

Table 3. Comparison of the geometric and thermodynamic parameters of an air-based (HPES-1) and a CO₂-based (HPES-2) system.

Parameter (Unit)	HPES-1	HPES-2
Compressible fluid	Air	CO ₂
Peak pressure— p_f (bar)	57.30	57.30
Initial pressure— p_0 (bar)	38.20	38.20
Accumulator length— L (m)	150	150
Accumulator outer diameter— D_o (m)	1.524	1.524
Accumulator inner diameter— D_{in} (m)	1.49	1.49
Accumulator wall thickness— e_w (mm)	17.06	17.06
Volumetric capacity— V_c (m ³)	261	261
Mass of steel— m_s (t)	95	95
Mass of working fluid— m_{air} or m_{CO_2} (t)	7	24
Ideal ESC— ESC_i (kWh)	148	320

The operating pressure and temperature were limited to the subcritical conditions of CO₂ as per the pressure–enthalpy plots [21] which allowed the fluid to undergo phase change. The length L and outer diameter D_o of the accumulator for both systems were kept

constant throughout, thus also resulting in an identical volumetric capacity V_c . For HPES-2, the mass of CO_2 is higher than the mass of air requirement in HPES-1, due to the lower density of the former fluid. The 24 tonnes (t) needed in HPES-2 is equivalent to simply 0.16% of the CO_2 emissions resulting from a total of 2034 private flights departing from Malta in 2022 [22].

Table 3 further lists the ideal ESC of both HPES systems. The value of 320 kWh for HPES-2 represents the maximum theoretical ESC_i at an r_p of 1.5 (marked in Figure 4a with a red circle). In other words, the ESC_i value reflects isothermal conditions, with CO_2 reaching a dryness fraction x of zero (i.e., full liquefaction). However, Figure 4a illustrates how the ESC_i varies linearly with the value of x . The higher the mass of CO_2 that manages to turn into a liquid (or the lower the value of x), the more energy is stored. Moreover, the lower the value of r_p (or the higher the value of the pre-charge pressure p_0 for a given p_f), the higher the ESC that can be attained.

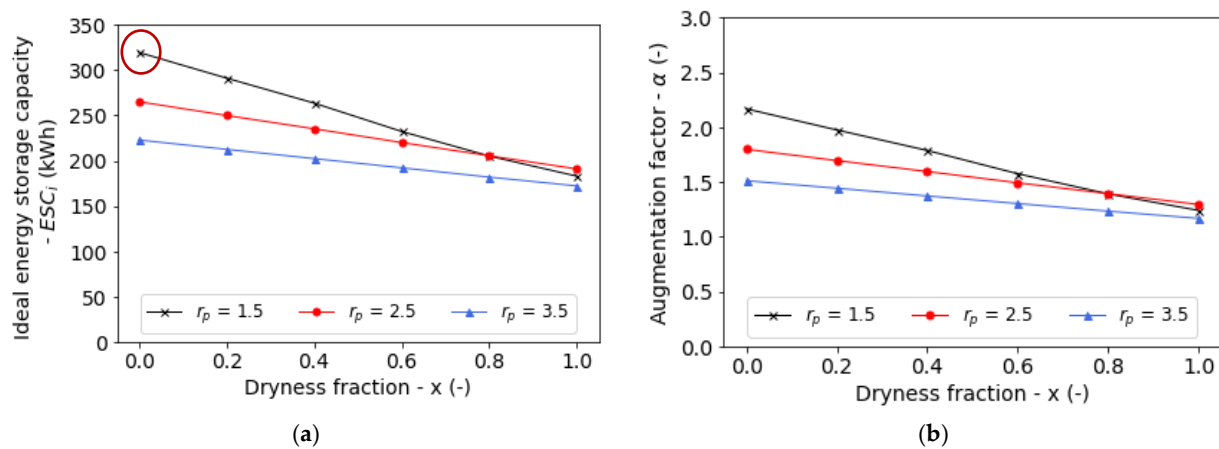


Figure 4. Potential increase in the ESC of a subsea HPES system when using CO_2 in lieu of air. (a) Variation of theoretical ideal ESC with dryness fraction of CO_2 for different pressure ratios. (b) Variation of augmentation factor with dryness fraction of CO_2 for different pressure ratios.

In a similar manner, Figure 4b demonstrates the increase in α with a reduction in the value of x , which is also a linear relationship. Considering all test cases, the ESC (in kWh) of HPES-2 relative to that of HPES-1 can be augmented by a factor ranging between 1.17 and 2.17. The ESD (in kWh/m^3) thus augments by the same factor, given that there are no geometric differences between the accumulator of HPES-1 and HPES-2. The magnitude of α depends on the test conditions, mainly r_p and x . For example, in the worst-case scenario with an r_p of 3.5, CO_2 remains in a gaseous state (i.e., $x = 1$) and the increase in ESC is minimal, with α equating to 1.17. Conversely, lowering r_p to 1.5 and increasing x such that more than 80% of the mass of CO_2 is liquefied can more than double the ESC and/or ESD of the HPES system.

4.2. Results from Transient Thermal Analysis

The conditions for the tests performed simulating transient thermal effects, taking into account the thermal resistance to heat transfer between the compressible fluid storing energy (i.e., CO_2) and the surrounding seawater, are given in the first five columns of Table 4. The latter indicates how r_p , T_0 , and t were varied, one at a time to assess the influence of every parameter on the ideal and real ESCs of HPES-2, as well as the thermal efficiency η and the ESC factor β . Indeed, the outcomes for ESC_i (CO_2), ESC_r (CO_2), η and β are given in the same table for every corresponding test. Note also how the dis/charging periods were maintained higher than 6 h to simulate LDES conditions. Test G is an exception where t was limited to 3 h to investigate the effect of short dis/charging periods.

Table 4. Test conditions of and outcomes from the transient thermal analysis for the CO₂-based HPES-2.

Test	HDPE Liner (-)	Initial Temp T ₀ (K)	Pressure Ratio r _p (-)	Dis/Charging Time t (h)	Ideal ES C ¹ ESC _i (kWh)	Real ES C ² ESC _r (kWh)	Efficiency η (-)	ESC Factor β (-)
A	No	293.15	1.5	6	320	160	0.9081	0.5056
B	No	293.15	2.5	6	262	177	0.9151	0.6778
C	No	293.15	3.5	6	220	161	0.9074	0.7337
D	No	283.15	1.5	6	260	248	0.8591	0.9519
E	No	288.15	1.5	6	288	166	0.8752	0.5774
F	No	298.15	1.5	6	340	149	0.9109	0.4369
G	No	293.15	1.5	3	320	150	0.8437	0.4765
H	No	293.15	1.5	12	320	165	0.9467	0.5240
I	No	293.15	1.5	24	320	169	0.9690	0.5351
J	No	283.15	1.5	24	260	234	0.9648	0.8973
K	Yes	293.15	1.5	6	285	131	0.8293	0.4584
L	Yes	283.15	1.5	24	235	178	0.2255	0.7580

¹ Obtained from thermodynamic model CO2HPES [12]. ² Obtained from transient thermal model C₂O₂ [6].

All tests (i.e., Tests A and L) were conducted to account for the presence of a bi-directional PIG with the design parameters listed in Table 5. The size of the PIG was selected based on market-ready solutions [23]. The diameter of the seal discs was chosen to be slightly larger than the inner diameter D_{in} of the accumulator, as described in Table 3. Made from a polymeric material, the discs are allowed to bend and fit inside the accumulator, whilst creating a seal to properly separate the CO₂ from the seawater inside the system. For a specified number of simulations (i.e., Tests K and L), the presence of the HDPE liner was also incorporated. The liner properties are listed in Table 6, with the liner thickness value chosen after a preliminary study.

Table 5. Design parameters of bi-directional PIG.

Parameter (Unit)	Value	Source
Disc diameter—D _d (m)	1.50	[23]
Disc thickness—e _d (m)	0.04	[23]
Static friction coefficient—μ _s (-)	0.60	[24]
Kinetic friction coefficient—μ _k (-)	0.50	[24]

Table 6. Properties of HDPE liner included in Tests K and L.

Parameter (Unit)	Value	Source
Density—ρ _l (kg/m ³)	948	[25]
Thermal conductivity—k _l (W/m K)	0.40	[25]
Specific heat capacity—c _l (J/kg K)	1810	[25]
Liner thickness—e _l (m)	0.036	
Liner roughness—ε _l (m)	0.000005	[25]

Table 4 indicates the maximum ESC_i of the system derived from the CO2HPES model [12] and Equation (6) as outlined in Section 2.1. The values are thus representative of ideal isothermal conditions, with fully liquefied CO₂ at the end of the charging process (i.e., x = 0). The ESC_r magnitudes are the values derived from the transient thermal simulations representing real conditions performed using the C₂O₂ model [6] as described in Section 2.2 (refer to Equations (8) and (10)).

For every test, the charging–hold–discharging–hold cycle is superimposed on the p–h plots of Figures 5–11, which also indicate the saturated liquid and saturated vapour CO₂ lines. The two lines create what can be referred to as a dome-like region: the region which indicates the two-phase transition of CO₂. The fluid is fully liquefied if it reaches the conditions specified by the saturated liquid line on the left-hand side of the plots. Outside the dome, the right-hand side region beyond the saturated vapour line signifies superheated CO₂ gas.

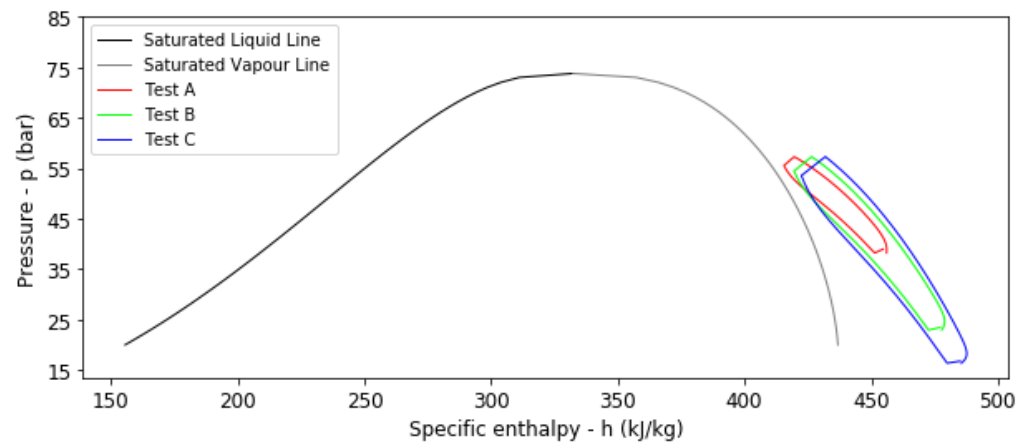


Figure 5. The p-h plot for Tests A, B, and C showing the state of CO₂ during operation for different operating pressure ratios r_p .

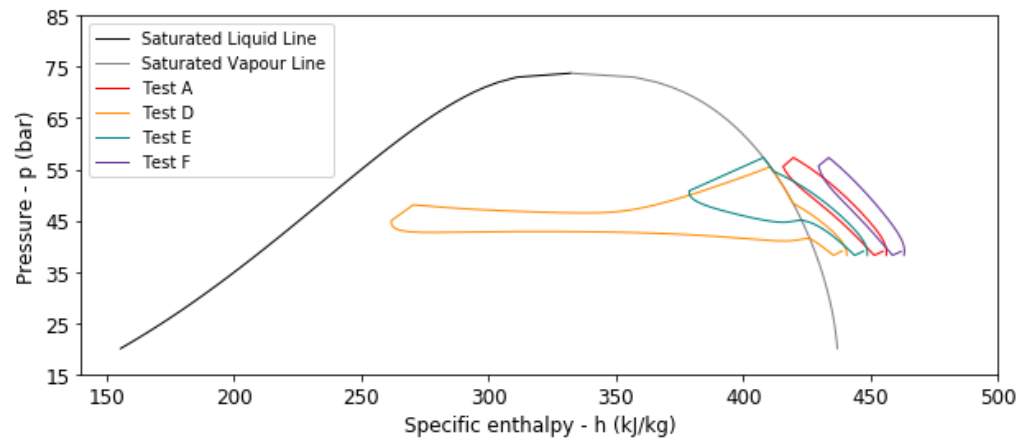


Figure 6. The p-h plot for Tests A, D, E, and F showing the state of CO₂ during operation for different initial temperatures T_0 .

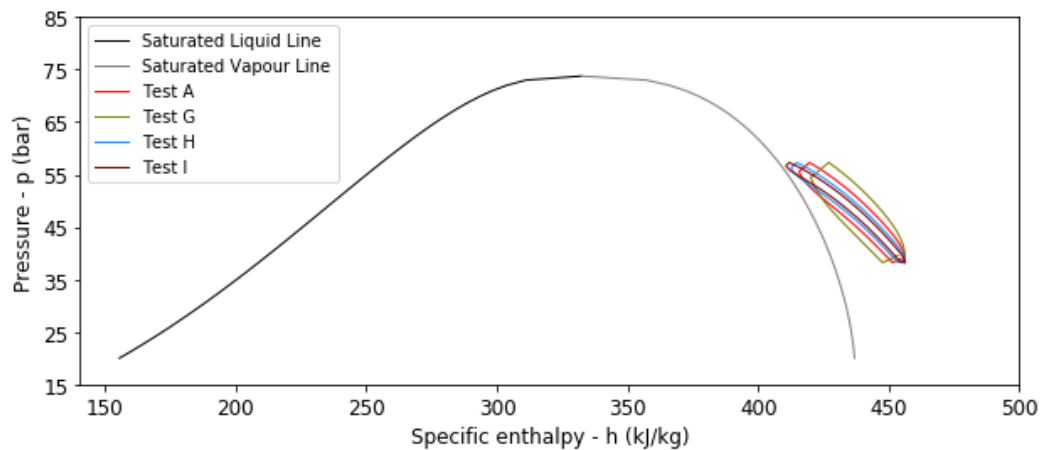


Figure 7. The p-h plot for Tests A, G, H, and I showing the state of CO₂ during operation for different dis/charging periods t at an initial temperature T_0 of 293.15 K.

Firstly, Figure 5 compares Tests A to C, thus reflecting any variations due to a distinct r_p (or p_0). The figure reveals that, in all three cases, the CO₂ does not manage to change phase. Indeed, despite η values above 0.90 (refer to Table 4) due to narrow hysteresis loops, the real ESC_r is low as compared to the ideal ESC_i . Moreover, the magnitudes in Table 4

suggest that r_p does not have a significant influence on the efficiency η . On the other hand, higher values of r_p , or smaller values of p_0 , result in better β values.

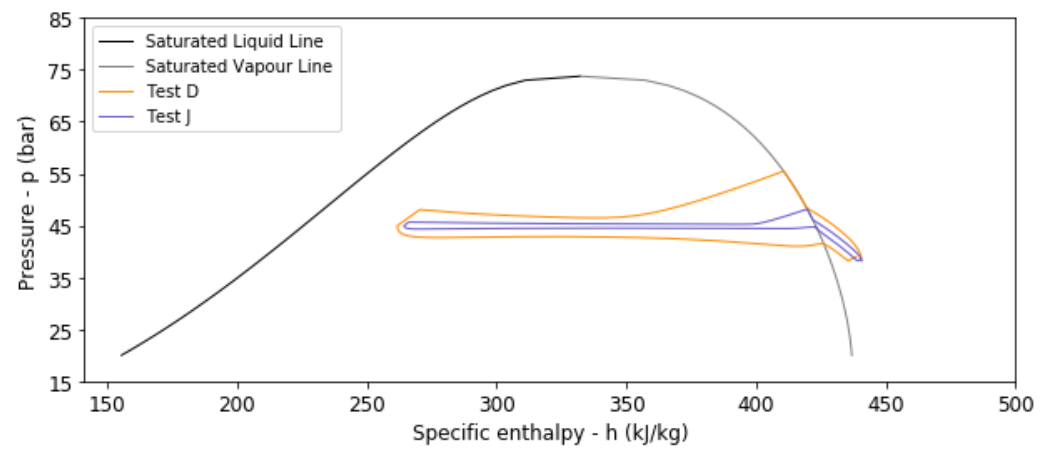


Figure 8. The p-h plot for Tests D and J showing the state of CO₂ during operation for different dis/charging periods t at an initial temperature T_0 of 283.15 K.

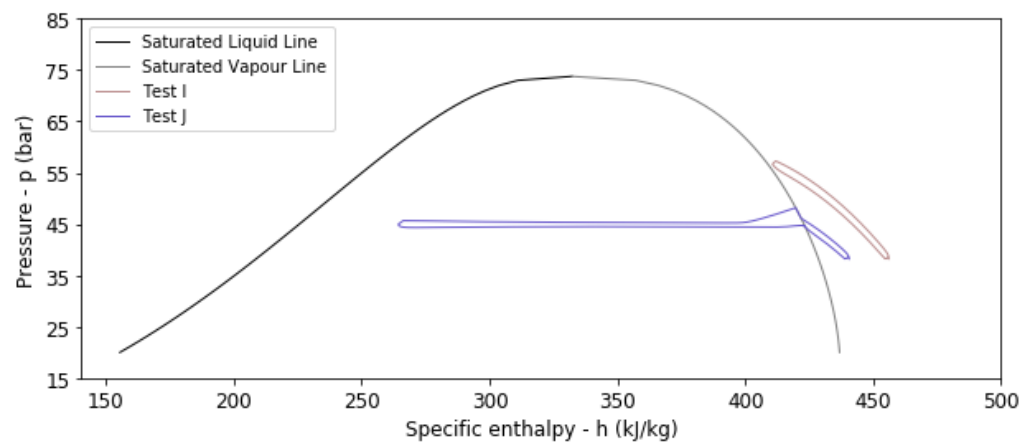


Figure 9. The p-h plot for Tests I and J showing the state of CO₂ during operation for different initial temperatures T_0 at a dis/charging period t of 24 h.

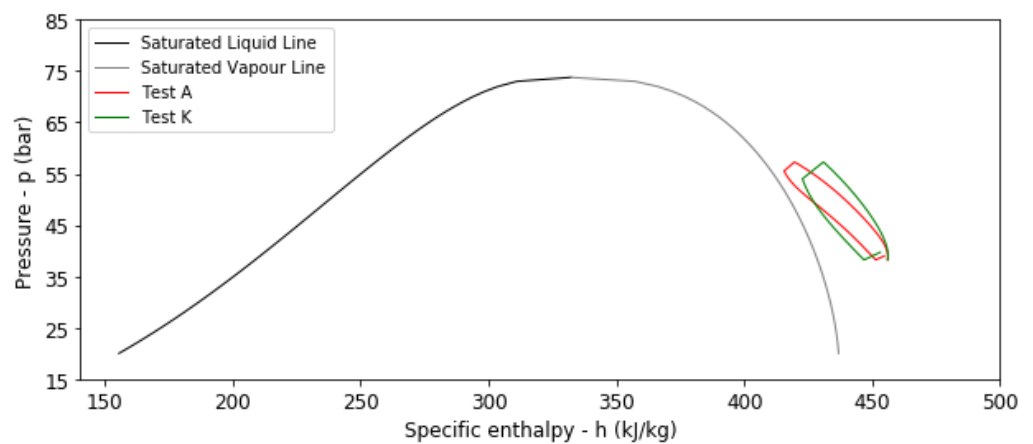


Figure 10. The p-h plot for Tests A and K showing the state of CO₂ during operation with and without HDPE liner at an initial temperature T_0 of 293.15 K and a dis/charging period t of 6 h.

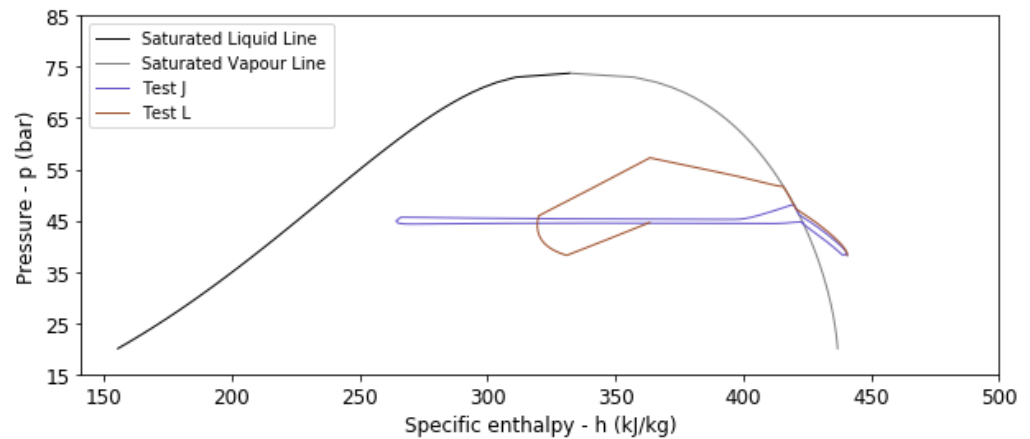


Figure 11. The p-h plot for Tests J and L showing the state of CO₂ during operation with and without HDPE liner at an initial temperatures T_0 of 283.15 K and a dis/charging period t of 24 h.

The effect of initial temperature T_0 on the operation of HPES-2 is visualized in Figure 6. The latter suggests that for the modelled conditions, the CO₂ changes phase only for T_0 values lower than 288.15 K. Referring to the outcomes in Table 4, the η values for Tests A, D, E, and F all exceed 0.85. Yet, an exceptional ESC factor β of 0.95 is only recorded for Test D, when 80% (i.e., $x = 0.20$) of the mass of CO₂ in the system liquefies prior to the first hold period.

The outcomes from Tests A, G, H, and I are superimposed on Figure 7. The latter confirms that longer dis/charging durations result in smaller hysteresis loops, and thus more efficient operating cycles, as may also be realized from the corresponding η values in Table 4. Yet, increasing the dis/charging period does not contribute to CO₂ liquefaction. For example, doubling the dis/charging duration from 12 to 24 h improves β by simply 2%. Indeed, the average β value for Tests A, G, H, and I, equates to 0.51, thus implying that augmenting the operating period up to 24 h still leaves half of the system's capacity untapped. Comparing Tests D and J in Figure 8 is an alternative approach to isolating the effect of dis/charging period at an initial temperature T_0 which permits CO₂ to enter the transition region. The magnitude of η for Test J is higher than that recorded for Test D due to lengthier dis/charging periods. Indeed, the hysteresis effect for Test J is much smaller than that observed for Test D. Nonetheless, both η and β for Tests D and J exceed 0.85 as CO₂ liquefies to low dryness fractions (i.e., $x \approx 0.20$).

Figure 9 depicts the difference between Tests I and J, verifying that T_0 governs the phase change of CO₂, and thus the β value. Indeed, with reference to Table 4, the outcomes of η for both scenarios are very similar. Yet, the β magnitude increases by 68% from Tests I to J, as a substantial amount of the gas is allowed to condense.

In Tests K and L, the effect of the HDPE liner is studied. Firstly, comparing Tests K to A via Table 4, it is evident that the liner reduces both η and β when CO₂ remains in the gaseous phase. Figure 10 further confirms the digitized outcomes, as a larger (i.e., wider) cycle is observed for Test K on the p-h plot. Analyzing Tests J and L in Figure 11 uncovers the effect of the liner when CO₂ does not remain in the gaseous phase. Despite the presence of the liner, CO₂ still liquefies under the conditions prescribed in Test L. Yet, the liner causes the path on the p-h plot to be very particular and to substantially deviate from following an isotherm. Interestingly, after 24 h of discharge, the CO₂ under the conditions of Test L does not return back to the initial state, as has been observed with Test J in the absence of the liner, and all other tests in Figures 5–10. Indeed, the plot for Test L in Figure 11 does not complete a closed cycle. Upon complete discharge, the CO₂ cools down to the initial temperature of 283.15 K. Yet, the pressure drop down to 44.6 bar (rather than 38.2 bar) retains 30% of the mass of CO₂ in a liquid state. Thus, the η value diminishes to 0.22.

5. Conclusions

Through numerical modelling, this study has unravelled the opportunities and challenges arising from the use of CO₂ as the energy storage medium in a subsea HPES system. Thermodynamic and transient thermal analyses have established that maintaining subcritical operating conditions and allowing CO₂ to undergo a phase change can provide multiple benefits. The following could be concluded:

- In an ideal scenario, where the CO₂ gas is completely liquefied and the phase change process follows an isothermal path, the ESC (or ESD) of the HPES system operating at a peak pressure of 57.3 bar can be increased by a maximum augmentation factor α , of 2.17;
- The magnitude of α depends on multiple aspects including the dryness fraction x and the pressure ratio r_p ;
- The minimum α value of 1.17 has been achieved at an r_p value of 3.5 and an x value of unity.

Notwithstanding the key benefits listed in the previous paragraph, operation on CO₂ in lieu of air also presents a number of limitations:

- Being limited to operate below the critical pressure of 73.8 bar limits the augmentation factor α that can be achieved;
- Transient thermal modelling that takes into account the resistance to heat transfer between the CO₂ and the surrounding seawater has indicated that under certain conditions, the real operating cycle deviates appreciably from the ideal, isothermal scenario, resulting in instances when the CO₂ remains in a gaseous state. Thus, despite a value of η beyond 0.90 being achievable, the ESC still remains significantly low;
- Simulations have also revealed that, for the test cases considered, operation of HPES-2 must be maintained below 288.15 K for CO₂ to enter the transition region;
- Adding on to the previous point, the initial operating temperature T_0 has been noted to be the main controlling parameter in determining whether the CO₂ undergoes a phase change during the storage cycle (gas–liquid–gas);
- A change in dis/charging duration has been observed to contribute to a change in the η value. Yet, it does not regulate the condensation and evaporation of CO₂;
- The presence of an HDPE liner reduces both the η and the β values.

Given the observations above, it is therefore important to emphasize that, when considering the operation of subsea HPES systems with CO₂ (or a fluid undergoing phase change), it is crucial to examine both the η and the β parameters. Unless the gas is allowed to liquefy in subcritical conditions, it will be impossible to achieve an ESC close to the ideal value. For the cases considered, an initial temperature T_0 of 283.15 K, a pressure ratio r_p of 1.5, and a dis/charging duration between 6 and 24 h were identified as optimal conditions to obtain both a η and a β value above 0.85.

The presented analysis thus provides motivation to explore in further depth the potential of subsea CO₂-based accumulators for energy storage applications. More comprehensive analysis incorporating measurements from scaled HPES systems in laboratory and/or subsea environments is necessary to validate the outcomes made known in this article. Thermal analysis utilizing alternative techniques as computational fluid dynamics (CFD) can provide further validation of the results laid forward in this study. Flow visualization experiments and a better understanding of the chemical phenomena occurring during the two-phase state of the fluid will also assist in acknowledging aspects that might not be apparent through numerical modelling.

The conclusions drawn in the present study provide insight into how future research can improve the performance of a CO₂-based HPES system operating subsea. Evidently, regulating the initial and operating temperature is the main contributing parameter to obtain a high thermal efficiency combined with augmented ESC.

Author Contributions: Conceptualization, T.S.; methodology, C.C.; software, C.C. and L.J.B.; validation, C.C. and L.J.B.; formal analysis, C.C.; investigation, C.C.; resources, T.S.; data curation, C.C.;

writing—original draft preparation, C.C.; writing—review and editing, T.S. and L.J.B.; visualization, C.C.; supervision, T.S.; project administration, T.S.; funding acquisition, T.S. All authors have read and agreed to the published version of the manuscript.

Funding: The research presented in this article has been supported by two projects being funded by Xjenza Malta under the FUSION R&I Research Excellence Program: (1) SEA2F (Investigating the Thermal Performance of Subsea Energy Storage Accumulators with a 2-Phase Fluid Transition; project reference REP-2021-008) and (2) SAICOPES (Subsea Air Isothermal Compression using Offshore Pipelines in Long Duration Energy Storage Applications; project reference REP-2023-004).

Institutional Review Board Statement: Not applicable.

Informed Consent Statement: Not applicable.

Data Availability Statement: Data are contained within the article.

Conflicts of Interest: The authors declare no conflicts of interest. The funder had no role in the design of the study; in the collection, analyses, or interpretation of data; in the writing of the manuscript; or in the decision to publish the results.

References

1. Budt, M.; Wolf, D.; Span, R.; Yan, J. A Review on Compressed Air Energy Storage: Basic Principles, Past Milestones and Recent Developments. *Appl. Energy* **2016**, *170*, 250–268. [CrossRef]
2. Odukomaiya, A.; Abu-Heiba, A.; Graham, S.; Momen, A.M. Experimental and Analytical Evaluation of a Hydro-pneumatic Compressed-Air Ground-Level Integrated Diverse Energy Storage (GLIDES) System. *Appl. Energy* **2018**, *221*, 75–85. [CrossRef]
3. Enabling Large-Scale Offshore Energy Storage, FLASC—Renewable Energy Storage. Available online: <https://offshoreenergystorage.com/> (accessed on 11 July 2024).
4. Messer Group GmbH. *Properties of Carbon Dioxide*; Messer Group GmbH: Sulzbach, Germany.
5. Vecchi, A.; Li, Y.; Ding, Y.; Mancarella, P.; Sciacovelli, A. Liquid air energy storage (LAES): A review on technology state-of-the-art, integration pathways and future perspectives. *Adv. Appl. Energy* **2021**, *3*, 10047. [CrossRef]
6. Briffa, L.J.B.; Cutajar, C.; Sant, T.; Buhagiar, D. Numerical Modeling of the Thermal Behavior of Subsea Hydro-Pneumatic Energy Storage Accumulators Using Air and CO₂. *Energies* **2022**, *15*, 8706. [CrossRef]
7. Li, Y.; Yu, H.; Tang, D.; Li, Y.; Zhang, G.; Liu, Y. A Comparison of Compressed Carbon Dioxide Energy Storage and Compressed Air Energy Storage in Aquifers using Numerical Methods. *Ren. Energy* **2022**, *187*, 1130–1153. [CrossRef]
8. Sun, W.; Liu, X.; Yang, X.; Yang, X.; Liu, Z. Design and Thermodynamic Performance Analysis of a New Liquid Carbon Dioxide Energy Storage System with Low Pressure Stores. *Energy Convers. Manag.* **2021**, *239*, 114227. [CrossRef]
9. Zhang, Y.; Yang, K.; Hong, H.; Zhong, X.; Xu, J. Thermodynamic Analysis of a Novel Energy Storage System with Carbon Dioxide as Working Fluid. *Ren. Energy* **2016**, *99*, 682–697. [CrossRef]
10. CO₂ Battery, Energy Dome. Available online: <https://energydome.com/co2-battery/> (accessed on 20 July 2024).
11. Abu-Heiba, A.; Ally, M.R.; Smith, B.; Momen, A. Increasing Compressed Gas Energy Storage Density Using CO₂-N₂ Gas Mixture. *Energies* **2020**, *13*, 2431. [CrossRef]
12. Cutajar, C.; Sant, T.; Briffa, L.J.B.; Buhagiar, D. Assessing the potential increase in the energy storage density of subsea hydro-pneumatic accumulators using CO₂ in lieu of air. *J. Therm. Sci. Eng. App.* **2022**, *15*, 031001. [CrossRef]
13. Churchill, S.W.; Chu, H.H.S. Correlation Equations for Laminar and Turbulent Free Convection from a Horizontal Cylinder. *Int. J. Heat Mass Transf.* **1975**, *18*, 1049–1053. [CrossRef]
14. Churchill, S.W.; Bernstein, M.A. Correlating Equation for Forced Convection from Gases and Liquids to a Circular Cylinder in Crossflow. *J. Heat Transf.* **1977**, *99*, 300–306. [CrossRef]
15. Ludovisi, D.; Garza, I.A. Natural Convection Heat Transfer in Horizontal Cylindrical Cavities: A Computational Fluid Dynamics (CFD) Investigation. In Proceedings of the ASME 2013 Power Conference, Boston, MA, USA, 29 July–1 August 2013.
16. Gnielinski, V. New Equations for Heat and Mass Transfer in Turbulent Pipe and Channel Flow. *Int. Chem. Eng.* **1976**, *16*, 359–368.
17. Thome, J.; El Hajal, J.; Cavallini, A. Condensation in horizontal tubes, part 2: New heat transfer model based on flow regimes. *Int. J. Heat Mass Transf.* **2003**, *46*, 3365–3387. [CrossRef]
18. Fang, X. A new correlation of flow boiling heat transfer coefficients for carbon dioxide. *Int. J. Heat Mass Transf.* **2013**, *64*, 802–807. [CrossRef]
19. Welcome to Python.org, Python. Available online: <https://www.python.org/> (accessed on 25 July 2024).
20. Cutajar, C.; Sant, T.; Farrugia, R.N.; Buhagiar, D. A Software Tool for the Design and Operational Analysis of Pressure Vessels Used in Offshore Hydro-Pneumatic Energy Storage. *J. Energy Storage* **2021**, *40*, 102750. [CrossRef]
21. Download Mollier Charts, ChemicalLogic. Available online: <https://www.chemicallogic.com/Pages/DownloadMollierCharts.html> (accessed on 25 July 2024).
22. Committed to the Environment (CE). *CO₂ Emissions of Private Aviation in Europe*; Committed to the Environment (CE): Delft, The Netherlands, 2023.

23. Williamson, T.D. *Pipeline Services Pigging Products, Bulletin No: 3000.05.02*; TDW: Tulsa, OK, USA, 2017.
24. Zhu, X.; Zhang, S.; Li, X.; Wang, D.; Yu, D. Numerical simulation of contact force on bi-directional pig in gas pipeline: At the early stage of pigging. *J. Nat. Gas Sci. Eng.* **2015**, *23*, 127–138. [[CrossRef](#)]
25. Canada's Oil and Natural Gas Producers (CAPP). *Use of High Density Polyethylene (HDPE) Lined Pipelines*; Canada's Oil and Natural Gas Producers (CAPP): Calgary, AB, Canada, 2022.

Disclaimer/Publisher's Note: The statements, opinions and data contained in all publications are solely those of the individual author(s) and contributor(s) and not of MDPI and/or the editor(s). MDPI and/or the editor(s) disclaim responsibility for any injury to people or property resulting from any ideas, methods, instructions or products referred to in the content.